Materials and Design 196 (2020) 109094

Contents lists available at ScienceDirect

Materials and Design

journal homepage: www.elsevier.com/locate/matdes

3D printing of PVA/hexagonal boron nitride/bacterial cellulose composite scaffolds for bone tissue engineering

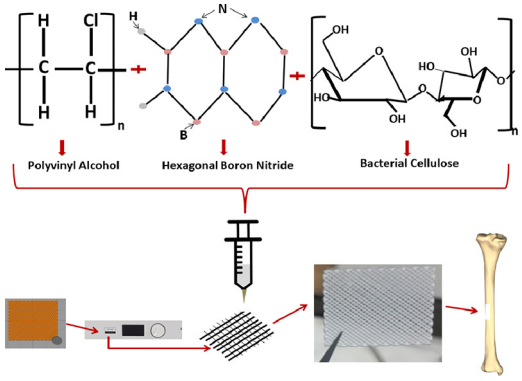
Deniz Aki [a,b], Songul Ulag [a,b], Semra Unal [a,c], Mustafa Sengor [a,b,*], Nazmi Ekren [a,d], Chi-Chang Lin [e], Hakan Yılmazer [f], Cem Bulent Ustundag [g], Deepak M. Kalaskar [h,**], Oguzhan Gunduz [a,b]

[a] Center for Nanotechnology & Biomaterials Application and Research (NBUAM), Marmara University, Turkey
[b] Metallurgical and Materials Engineering, Marmara University, Turkey
[c] Bioengineering, Institute of Pure and Applied Sciences, Marmara University, Turkey
[d] Electrical and Electronics Engineering, Faculty of Technology, Marmara University, Turkey
[e] Chemical and Materials Engineering, Tunghai University, Taiwan
[f] Department of Bioengineering, Faculty of Chemistry and Metallurgy, Yildiz Technical University, Turkey
[g] Department of Metallurgical and Materials Engineering, Yildiz Technical University, Turkey
[h] Institute of Orthopedics & Musculoskeletal Science, Division of Surgery and Interventional Science, Royal National Orthopedic Hospital, University College London, UK

HIGHLIGHTS

- 3D printed PVA with hexagonal boron nitride and bacterial cellulose were promising for bone tissue engineering applications.
- Bacterial cellulose was obtained successfully from *Gluconacetobacter xylinus*.
- Scaffolds with controlled porosity were fabricated.
- Additive manufacturing used for scaffold production.

GRAPHICAL ABSTRACT



ARTICLE INFO

Article history:
Received 29 May 2020
Received in revised form 5 August 2020
Accepted 22 August 2020
Available online 30 August 2020

Keywords:
Bacterial cellulose
Bone tissue engineering
Hexagonal boron nitride
Osteoblast cell line
Polyvinyl alcohol
3D bioprinting

ABSTRACT

In this study, a novel Polyvinyl Alcohol (PVA)/Hexagonal Boron Nitride (hBN)/Bacterial Cellulose (BC) composite, bone tissue scaffolds were fabricated using 3D printing technology. The printed scaffolds were characterized by fourier transform infrared spectroscopy (FT-IR), scanning electron microscopy (SEM), tensile testing, swelling behaviour, differential scanning calorimetry (DSC), and in vitro cell culture assay. Results demonstrated that bacterial cellulose addition affected the characteristic properties of the blends. Morphological studies revealed the homogenous dispersion of the bacterial cellulose within the 12 wt%PVA/0.25 wt%hBN matrix. Tensile strength of the scaffolds was decreased with the incorporation of BC and 12 wt%PVA/0.25 wt%hBN/0.5 wt%BC had the highest elongation at break value (93%). A significant increase in human osteoblast cell viability on 3D scaffolds was observed for 12 wt%PVA/0.25 wt%hBN/0.5 wt%BC. Cell morphology on composite scaffolds showed that bacterial cellulose doped scaffolds appeared to adhere to the cells. The present work deduced that bacterial cellulose doped 3D printed scaffolds with well-defined porous structures have considerable potential as a suitable tissue scaffold for bone tissue engineering (BTE).

* Corresponding author at: Center for Nanotechnology & Biomaterials Application and Research (NBUAM), Marmara University, Turkey.
** Corresponding author.
E-mail addresses: mustafa.sengor@marmara.edu.tr (M. Sengor), d.kalaskar@ucl.ac.uk (D.M. Kalaskar).

https://doi.org/10.1016/j.matdes.2020.109094
0264-1275/© 2020 The Author(s). Published by Elsevier Ltd. This is an open access article under the CC BY license (http://creativecommons.org/licenses/by/4.0/).

© 2020 The Author(s). Published by Elsevier Ltd. This is an open access article under the CC BY license (http://creativecommons.org/licenses/by/4.0/).

1. Introduction

Bone has the responsibility within the body to offer mechanical support and flexibility, consists of 60% mineral, 30% organic component, and 10% water [1]. Bone can be classified as trabecular bone and cortical bone. Trabecular bone provides the movement of limbs, and joints and cortical bone supplies mechanical support and protective shield. For the treatment of various defects resulting from tumours, trauma, infections and genetic malformations occurring in human bone, regeneration or healing of bone tissue is carried out with three-dimensional structures capable of mimicking the physical and chemical properties of the extracellular matrix (ECM) [2]. Bone grafting and transplantation is the current clinical assistance. There is an alternative to the conventional use of bone grafts which is engineered bone tissues. Tissue-engineered bone has a limitless supply, and it does not allow disease transmission. However, there are some limitations or difficulties in terms of clinical practice. To overcome these challenges, bone tissue engineering (BTE) aims to regenerate bones via combination of cells, biomaterials and factor therapy [3]. BTE has become one of the favourite areas to facilitate bone regeneration and the treatment of diseased or damaged tissues. BTE leads regeneration of targeted tissues by combining osteoconductive scaffolds, osteogenic cells, and osteoinductive signals.

Tissue-engineered scaffolds enable cells attachment and effective tissue regeneration. Thus, tissue-engineered scaffolds should have necessary properties, which are biocompatibility, biodegradability, proper mechanical properties, and interconnected porous structures. Fabrication technique also has a critical effect on the properties of the aimed artificial scaffolds. There are some traditional fabrication methods such as gas foaming, freeze-drying, fiber bonding, particulate/salt leaching, emulsification and phase separation/inversion [4]. These methods may have some problems with the control of the geometry, porosity and pore shape. 3D printing is a novel method to overcome these disadvantages of traditional methods. This new technology has been used to build scaffolds with designed shapes and porosity which leads to improved cell growth and regeneration [5,6]. The results of the 3D printing process demonstrate superior properties with adjustable porosity and mechanical strength [7].

Li et al. analyzed the boron nitride addition into the PVA matrix to obtain the BN/PVA composites using cyclic freezing and thawing method. They reported that hBN addition improved the mechanical properties of the composites.

Moreover, hBN addition also increased the thermal stability and swelling degree of the composite hydrogels [8]. Zaboroska et al. study investigated both nanoporous and microporous bacterial cellulose effect on NC3T3-E1 osteoprogenitor cells. This work, also reported that microporous BC is a promising biomaterial for bone tissue regeneration [9]. The effect of varying composition of PVA, hexagonal boron nitride and bacterial cellulose have been studied separately for bone tissue engineering. Still, no previous studies have been reported using these polymers together to obtain bone tissue scaffold.

In this study, 3D bioprinting technology was managed to produce 3D porous bone scaffolds that are compatible with bone physical and mechnanical structure, using polyvinyl alcohol (PVA)-hexagonal boron nitride (hBN)-bacterial cellulose (BC) polymeric blends to get an ideal scaffold for effective bone healing. The amount of bacterial cellulose in PVA/hBN matrix was investigated with different BC contents due to its superior biocompatible properties, crystallinity, non-toxicity, and hydrophilicity [10]. It has outstanding effects on cell adhesion with its interconnected porous structure [11,12]. PVA can provide desirable flexibility, hydrophilicity, outstanding chemical stability, and semi-permeability to the scaffolds as host material, which are crucial for transporting oxygen and nutrients for cell survival [13]. The hBN has been used as fillers due to its excellent thermal conductivity, thermal stability, and superior mechanical properties. Additionally, hBN has been used in biomedical applications as a promising material due to its excellent biocompatibility property.

2. Materials and methods

2.1. Materials

Polyvinyl alcohol (MW = 89,000–98,000) was purchased from Sigma Aldrich, USA. Hexagonal Boron Nitride (APS < 1 μm) was obtained from American Elements. Acetic acid glacial (MW = 60.05) with 99.7% purity was purchased from VWR Chemicals. Sodium hydroxide (NaOH, d = 40.00 g/mol) and D (+)-glucose anhydrous for biochemistry (M = 180.16 g/mol), and disodium hydrogen phosphate (MW = 141.96 g/mol, Na_2HPO_4) were purchased from Merck KGaA, Germany. Peptone from animal tissue from meat and citric acid (99% purity, MW = 192.12 g/mol) were purchased from Sigma Aldrich.

2.2. Method

2.2.1. Bacterial cellulose production by Gluconacetobacter xylinus

Gluconacetobacter xylinus was used to produce bacterial cellulose membranes (Fig. S1a). The bacterium was cultivated on Hestrin and Schramm (HS) medium consisted of 2.0 wt% D-glucose, 0.5 wt% peptone, 0.5 wt% yeast extract, 0.27 wt% disodium hydrogen phosphate and 0.115 wt% citric acid, and the pH at 5.0–6.0 with acetic acid. After incubating in a static incubator at 28 °C for 10 days, the BC membranes were purified by 0.1 M NaOH at 90 °C for 2 h and soaked them in deionized water (DI) several times. The samples were sterilized at 121 °C in an autoclave for 20 min, followed by oven-dried at 50 °C for 24 h. Oven-dried bacterial cellulose membranes were treated with 50% (v/v) sulphuric acid solution in a cellulose/acid ratio of approximately 20 g/L, at 50 °C for 2 h. The suspension was washed with deionized water and centrifuged and repeated until neutral pH (as shown in Fig. S1(b, c, d, e)).

2.2.2. Designing the 3D model and converting to the G-code

The 12 wt%PVA/0.25 wt%hBN and 12 wt%PVA/0.25 wt%hBN/(0.1, 0.25, and 0.5, wt%)BC composite scaffolds were fabricated using a 3D printing device (Ultimaker 2+ modified to hydrogel printer) which has heated build substrate and X-Y control head. This multifunctional machine was connected to the syringe pump to control the flow rate of the solutions, and the diameter value of the nozzle was 0.4 mm. The distance between the nozzle and substrate was adjusted to 0.03 mm. The scaffold model (20x20x5 mm^3) was designed with the Solidworks software, and this design was converted into the G-code via Simplify program, which provides to control the process parameters programmatically (Fig. 1 (a, b, c)).

2.2.3. Preparation of the 3D-printed 12 wt%PVA/0.25 wt%hBN/(0.1, 0.25, 0.5, wt%)BC composite scaffolds

Firstly, 12 wt% PVA was dissolved in distilled water (50 mL) and put on the magnetic stirrer in vials for 4 h at 90 °C to get a gel form of the PVA polymer. Then, the 0.25 wt%hBN powder was poured into the PVA solution. The concentration of BCs to the weight of PVA/hBN was 0.1, 0.25, and 0.5 wt%, respectively. Viscosity (Brookfield DV-E), surface tension (Sigma 700 DYNE) and density characteristics were obtained prior to printing (Table 1). In this work, several concentrations of PVA

solutions were used, but 12 wt%PVA was found best printable to form uniform pore distribution for determining optimum printable parameters with given parameters. After the PVA concentration was obtained, hBN particles were added into 12 wt%PVA matrix with a ratio of 0.25 wt% to increase the mechanical strength of the scaffolds. BC was added with three different rates to observe the BC effect on the properties of the scaffolds, especially cell viability and attachment. There was not used any chemical cross-linking agents to avoid their toxic effects. In the printing stage, 12 wt%PVA was fabricated at first, and the parameters during the printing process were 70% infill rate, 0.3 mL/h flow rate at room temperature. 12 wt%PVA/0.25 wt%hBN was printed with same infill rate as 12 wt%PVA, but 0.5 mL/h flow rate was reported for this stage. With the addition of 0.1, 0.25, 0.5 wt%BC into the 12 wt%PVA/0.25 wt%hBN, the value of flow rate was adjusted to 0.5, 0.8, and 1 mL/h, respectively. After whole scaffolds were obtained and dried at room temperature for 24 h, several characterization tests were performed to determine the properties of the printed scaffolds.

2.2.4. Physiochemical characterization of the 3D printed 12 wt%PVA/0.25 wt %hBN/(0.1, 0.25, 0.5, wt%) BC composites

Morphological and dimensional analyzes of the 3D composite scaffolds were accomplished by using scanning electron microscopy (SEM, EVO MA-10, Zeiss, Germany). Fourier Transform Infrared Spectroscopy (FT-IR) was used to analyze the presence of chemical groups between the components by using FT-IR-4700, Jasco which wavelength value ranges between 450 and 4000 cm^{-1}. Mechanical properties of the composite scaffolds were examined by using tensile test device (Shimadzu, Japan) with 5 kN load cell. Grup movement speed was adjusted to 5 mm/min, and two samples were selected for each concentration to increase the reliability of the tests. All test samples had the same width, Gauge length, and thickness values which were 15 mm, 6 mm, and 0.1 mm, respectively. Thermal properties of the scaffolds were determined by using DSC (Shimadzu) device in the closed pan, which shows the thermal transitions of the structures. Heating temperature ranges were adjusted from 25 to 550 °C, and the heating rate was selected at 10 °C/min. To prepare the scaffolds for SEM analysis, they were coated with gold for 90 s, 18 mA. The swelling behaviours of the composite scaffolds were tested with phosphate-buffered saline (PBS) for 7 days using thermo-shaker (BIOSAN) at 37 °C, 250 rpm. Before the swelling degree measurement, the dry weight of the scaffolds was measured and recorded. After that, they were placed in eppendorf tubes with PBS. Dry measurements were taken each day and after composite scaffolds were wiped with filter paper to remove the saline on the surface. The swelling degrees of the composite scaffolds were calculated with the formula used in the Li et al. study [8].

2.2.5. In vitro tests of the 3D printed 12 wt%PVA/0.25 wt%hBN/(0.1, 0.25, 0.5, wt%) BC composites

The human osteoblast cell line (from American Type Culture Collection (ATCC)) was used for all cell experiments in growth medium (Dulbecco's modified eagle's medium (DMEM) supplemented with 10% fetal bovine serum (FBS) and 1% penicillin/streptomycin. Printed bone tissue composite scaffolds were cut to a diameter of 6 mm and then placed into 96-well plates, followed by ultraviolet (UV) light sterilization for 2 h. Cell suspension with 1×10^4 cells per well was cultured on the printed composite scaffolds and cell plate (2D) and then incubated at 37 °C and 5% CO_2 for 72 h. MTT [3- (4,5-dimethyldiazol-2-yl) -2,5 diphenyl tetrazolium bromide] protocol was applied in order to detect cell viability in our material. After incubation, the cell medium was removed and then 0.2 mL of 0.5 mg/mL MTT in PBS was added to each well, followed by incubated for 4 h at 37 °C with 5% CO_2. The supernatant was removed gently, followed by the addition of dimethylsulfoxide (DMSO). Then, each sample was transferred to a 96-well plate to measure the absorbance at 590 nm (reference 660 nm) wavelength using a microplate reader. In order to see the cell morphology on the composite scaffolds, the cells were fixed on the composite scaffold with 2.5% glutaraldehyde solution and purified by passing through a series of ethanol solutions (30%, 50%, 70%, 80%, 95%). The dried composite scaffolds

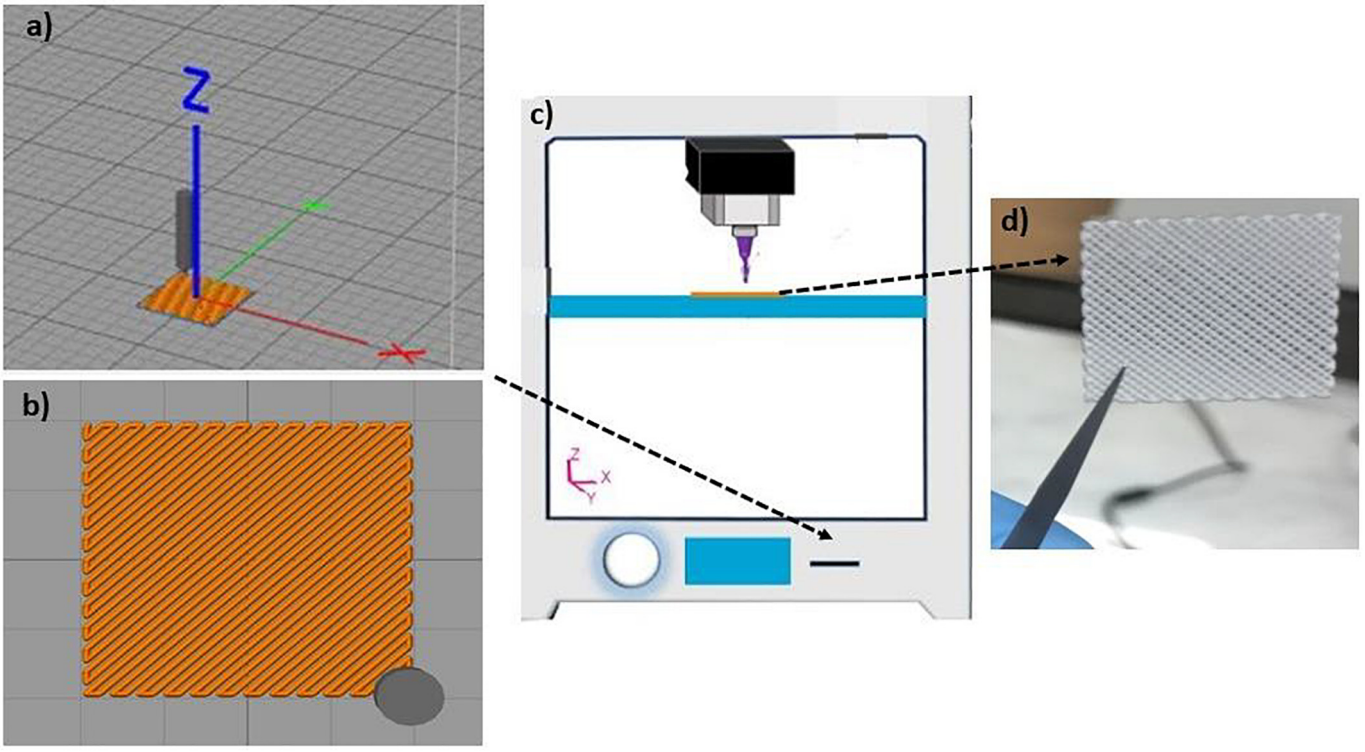


Fig. 1. Solid model of the composite and simulation of the printing process (a, b), representative image of the 3D printing device (c), image of the 3D-printed hexagonal boron nitride doped 12 wt%PVA matrix (d).

Table 1
Characteristics of the solutions and tensile testing results of the printed scaffolds.

Scaffolds	Viscosity (mPa.s)	Surface Tension (mN/m)	Density (g/mL)	Tensile Strength (MPa)	Elongation at break (%)
12 wt%PVA	50.9 ± 2.5	49 ± 5	1.01 ± 0.02	0.075 ± 0.05	48 ± 25
12 wt%PVA/0.25 wt%hBN	65 ± 4.0	50.3 ± 5	1.03 ± 0.002	0.12 ± 0.06	85 ± 28
12 wt%PVA/0.25 wt%hBN/0.1 wt%BC	71 ± 5	59.6 ± 5	1.05 ± 0.02	0.127 ± 0.05	80 ± 32
12 wt%PVA/0.25 wt%hBN/0.25 wt%BC	74.3 ± 6.5	64.3 ± 5	1.06 ± 0.02	0.05 ± 0.05	65 ± 49
12 wt%PVA/0.25 wt%hBN/0.5 wt%BC	81.3 ± 4.5	65.3 ± 5	1.07 ± 0.02	0.1 ± 0.05	93 ± 23

were coated with a thin layer of gold (90 s) and examined at 10 kV using the SEM.

2.2.6. Statistical analysis

All data were demonstrated as the mean ± standart deviation. All experiments were carried out in duplicates. Their averages were taken as the final value and differences among groups were considered significant at $p < 0.05$.

3. Results and discussion

3.1. FTIR analysis

In Fig. 2A, pure PVA had absorption peaks at ~3279 cm^{-1} (-OH stretching), ~2905 cm^{-1} (C–H stretching), ~1417 cm^{-1} (C–O group), ~1323 cm^{-1} (C–H bending), ~1237 cm^{-1} (C═O vibration), ~1140 cm^{-1} (C–O stretching), ~1086 cm^{-1} (C–O group), ~918 cm^{-1} (C–C stretching), ~832 cm^{-1} (C–O stretching) [14]. FTIR spectrum of the pure hBN revealed that it had two broad absorption peaks at ~1237.1 cm^{-1} and ~ 742.5 cm^{-1}. The peak at ~1237.1 cm^{-1} might be due to the B–N modes of the sp^2-bonded hBN and another peak at ~742.5 cm^{-1} might be due to the B-N-B out-of-plane bending vibration [15]. BC had broad absorption peaks at ~3340.1 cm^{-1}, which is due to the stretching of the –OH bond, another peak at ~2897 cm^{-1} refers to the stretching of the C–H bond. The peak at 1625 cm^{-1} attributed to the –OH of absorbed water. Another bending of planar CH observed at ~1316.2 cm^{-1}. Asymmetrical C-O-C stretching observed at ~1157.1 cm^{-1} [16]. In Fig. 2B (a), 12 wt%PVA composite had main absorption peaks at ~3268.8 cm^{-1} (O–H stretching), ~2906.2 cm^{-1}(antisymmetric stretching vibrational of C–H from alkyl groups), ~1416.5 cm^{-1} (CH_2 bending). Some differences can be detected between the 12 wt%PVA and 12 wt%PVA/0.25 wt%hBN FTIR spectrums. In Fig. 2B(b), FTIR spectra of the 12 wt%PVA/0.25 wt%hBN composite scaffolds had nearly the same spectrum with 12 wt%PVA but there were observed some shifts: the absorption peaks for 12 wt%PVA shifted slightly from ~834 cm^{-1} to ~832 cm^{-1}, ~916 cm^{-1} to ~917 cm^{-1}, ~1085 cm^{-1} to ~1084.8 cm^{-1}, ~1416 cm^{-1} to ~1413.6 cm^{-1}, ~2906.2 cm^{-1} to ~2909.1 cm^{-1} and ~ 3268.8 cm^{-1} to ~3253.3 cm^{-1}. These differences might be due to the interactions between the PVA and hBN particles. The peak at ~1141.7 cm^{-1} for 12 wt%PVA was not indicated in the 12 wt%PVA/0.25 wt%hBN composite scaffolds. In Fig. 2B (c), there was observed a similar tendency for 12 wt%PVA/0.25 wt% hBN/0.1 wt%BC except for the peak at ~1593.9 cm^{-1}. When compared to the peaks of the other spectrums, only one different peak (~1140.7 cm^{-1}) was observed for 12 wt%PVA/0.25 wt%hBN/0.25 wt% BC (Fig. 2B(d)). There were observed small shifts compared to the other spectrums for 12 wt%PVA/0.25 wt%hBN/0.5 wt%BC composite scaffolds, and one peak was only seen in this spectrum, which was absorbed in ~1647.9 cm^{-1} (Fig. 2B(e)).

3.2. SEM observations

SEM images of the composites were shown in Fig. 3 with labels. In Fig. 3a, 12 wt%PVA had a uniform structure and homogeneous pore distribution. The results indicated that the 3D printed composite scaffolds could be printed steadily over somewhat large

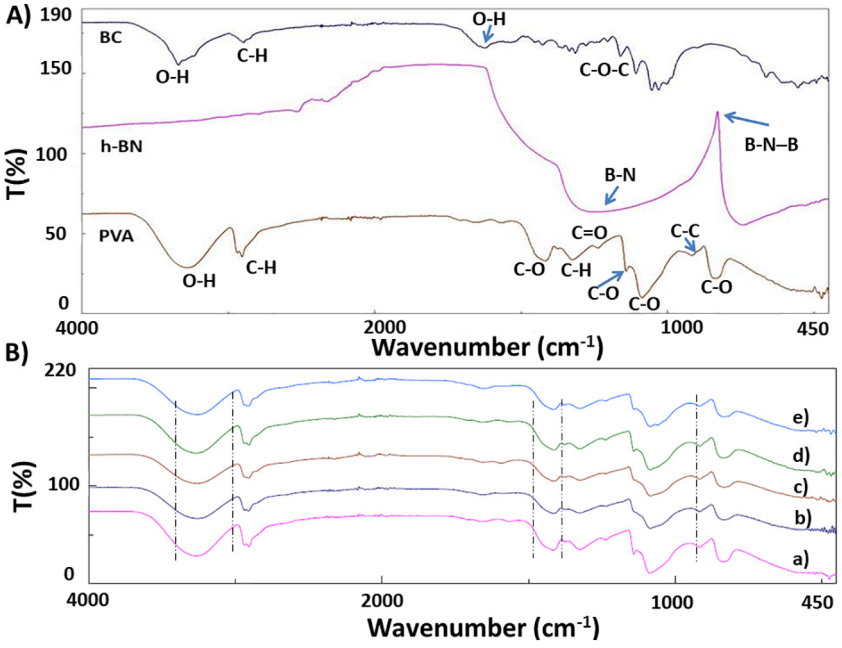


Fig. 2. FTIR spectrums of the pure polymers and synthesized BC (A), 12 wt%PVA (B, a), 12 wt%PVA/0.25 wt%hBN (B, b), 12 wt%PVA/0.25 wt%hBN/0.1 wt%BC (B, c), 12 wt%PVA/0.25 wt% hBN/0.25 wt%BC (B, d), 12 wt%PVA/0.25 wt%hBN/0.5 wt%BC (B, e).

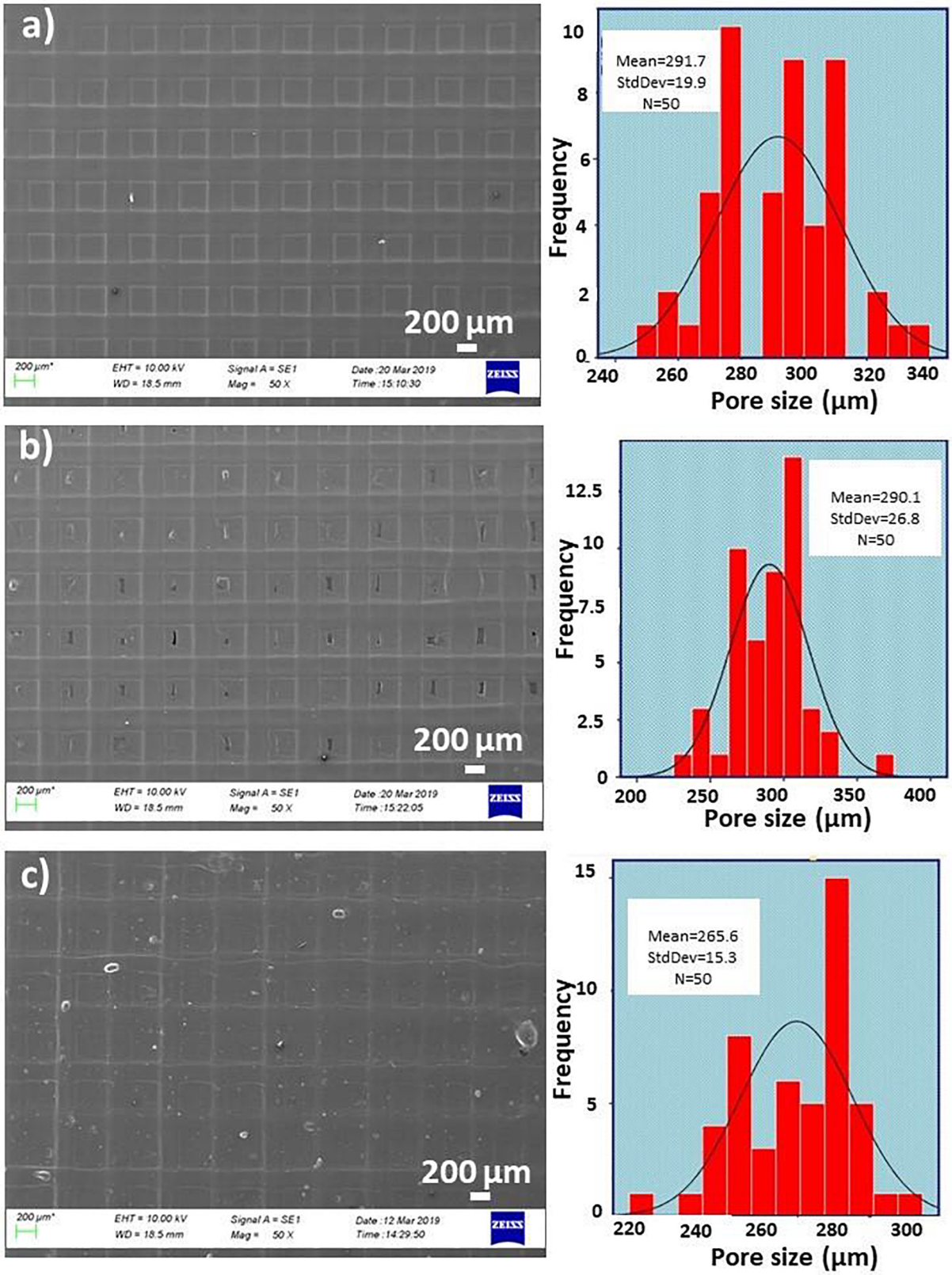


Fig. 3. SEM images of the 12 wt%PVA (a), 12 wt%PVA/0.25 wt%hBN (b), 12 wt%PVA/0.25 wt%hBN/0.5 wt%BC (c) with pore size histograms.

areas and heights [17]. The average pore size value was about 291.71 ± 19.94 µm. In Fig. 3b, 12 wt%PVA/0.25 wt%hBN composite scaffolds showed a relatively smooth surface, and its mean pore size value was 290.18 ± 26.80 µm. In Fig. 3c, with 0.5 wt%BC addition, 12 wt%PVA/0.25 wt%hBN/0.5 wt%BC had smaller pores of 265.68 ± 15.39 µm. In tissue engineering applications, pore size usually ranges from 150 to 500 µm [18–20]. It can be said that the pore size of synthesized scaffolds has a proper range of pore values to provide vascularization and nutrient transport for tissue engineering applications.

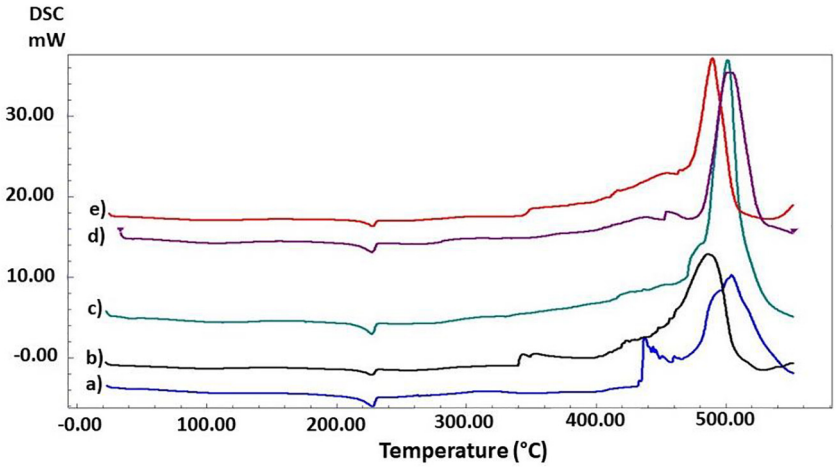


Fig. 4. DSC thermogram of the composite scaffolds: 12 wt%PVA (a), 12 wt%PVA/0.25 wt%hBN (b), 12 wt%PVA/0.25 wt%hBN/0.1 wt%BC (c), 12 wt%PVA/0.25 wt%hBN/0.25 wt%BC (d), 12 wt %PVA/0.25 wt%hBN/0.5 wt%BC (e).

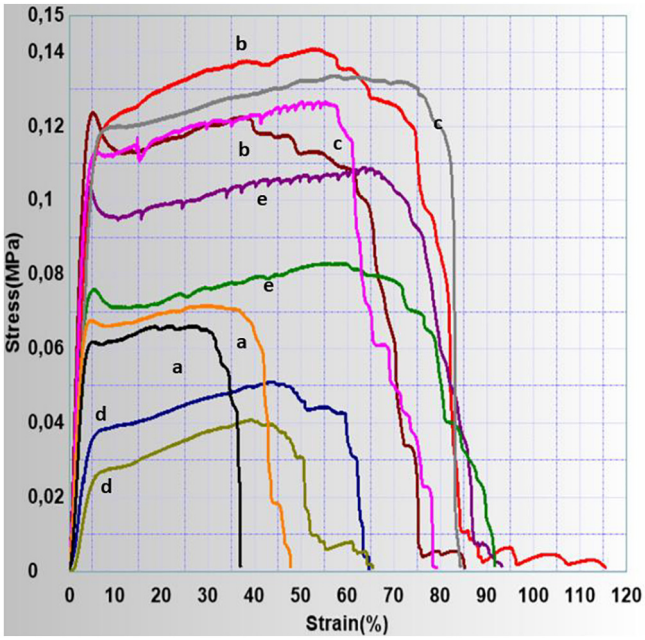


Fig. 5. Stress vs strain curve of 12 wt%PVA (a), 12 wt%PVA/0.25 wt%hBN (b), 12 wt%PVA/0.25 wt%hBN/0.1 wt%BC (c), 12 wt%PVA/0.25 wt%hBN/0.25 wt%BC (d), 12 wt%PVA/0.25 wt%hBN/0.5 wt%BC (e).

3.3. DSC thermographs

The Fig. 4 showed the DSC curves of 12 wt%PVA, 12 wt%PVA/0.25 wt %hBN and 12 wt%PVA/0.25 wt%hBN/(0.1, 0.25, 0.5, wt%)BC composite scaffolds in the temperature range 25–550 °C. The degree of crystallinity and water content in PVA effected the melting point. The melting point value for highly crystalline PVA is approximately 230 °C [21]. The melting point for our case was also very close to the 230 °C, which means our 3D printed 12 wt%PVA was highly crystalline. Incorporation of hBN and BC inside the host 12 wt%PVA resulted in a shift of this melting peak. Therefore, the crystallinity of the 12 wt%PVA was decreased with additive fillers [22]. On the other hand, the bare presence of PVA characteristic melting peaks on the curves of 12 wt%PVA/0.25 wt%hBN and 12 wt %PVA/0.25 wt%hBN/(0.1, 0.25, 0.5, wt%)BC blends did reveal the effect of additives on the PVA semi-crystallinity [23].

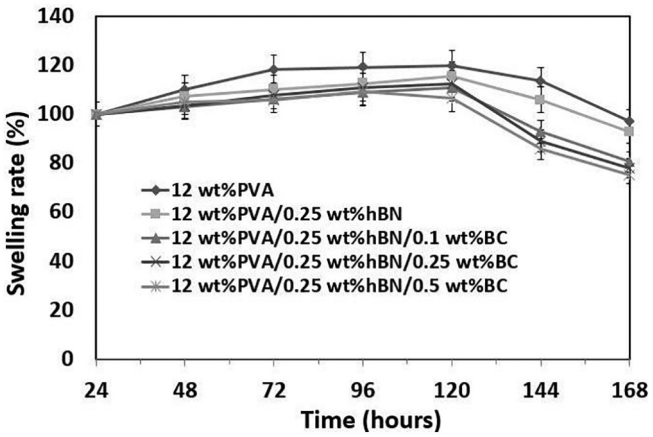


Fig. 6. Swelling degree graph for all composite scaffolds after one-week incubation.

3.4. Physico-chemical properties of the solutions

The physico-chemical properties of PVA, such as density, viscosity, and surface tension, are important parameters in the applications of PVA [24]. The physico-chemical properties of different BC-modified solutions were analyzed, as given in Table 1. It should be reported that the viscosity of the solution should be low enough to permit it to easily flow through the nozzle during the printing process, but also should be adequate to support the layer-by-layer construction structure. Furthermore, it is known that the viscosity of the solution can affect the connection of the pores [25]. The viscosity of the PVA solutions increased with the addition of hBN and BC concentration. There was observed 30% difference of viscosity value between the 12 wt%PVA and 12 wt%PVA/0.25 wt%hBN solutions. By adding 0.5 wt%BC into the matrix polymer, the viscosity values of the 12 wt%PVA/0.25 wt%hBN increased from 65 to 81.3 mPa.s. There was no significant difference between the density values of the solutions. The values changed from 1.01 g/mL (12 wt%PVA) to 1.07 g/mL (12 wt%PVA/0.25 wt%hBN/0.5 wt%BC). Table 1 also indicated that surface tension increased as the BC concentration increases and the maximum surface tension value (65 mN/m) observed for 12 wt%PVA/0.25 wt%hBN/0.5 wt%BC. According to the literature, surface tension is typically in the range of 30–70 mN/m [26], and the surface tension values of solutions found in this study were at this specified value ranges.

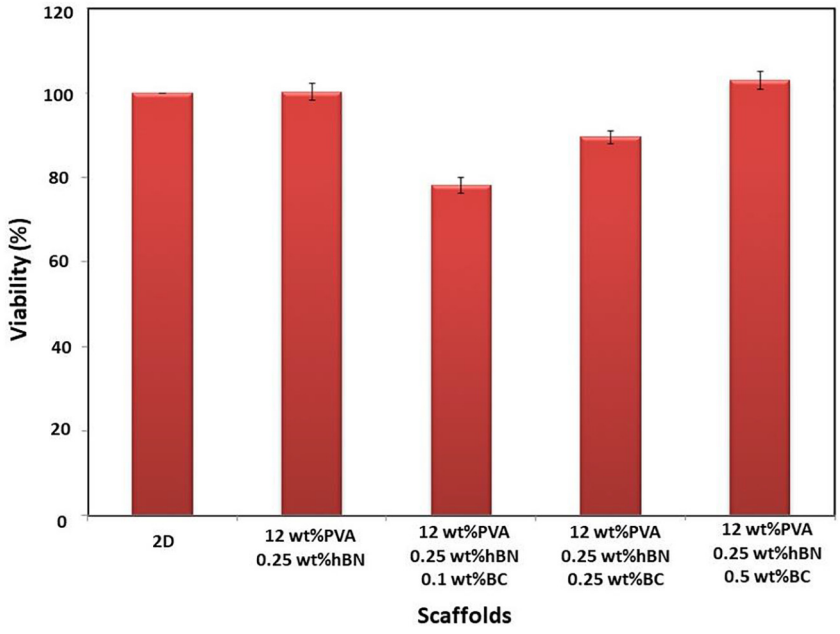


Fig. 7. Cell viability analysis of osteoblast on composite scaffolds with MTT assay.

3.5. Uniaxial tensile testing

The typical mechanical properties of the printed scaffolds like tensile strength and elongation at break values were listed in Table 1 and showed in Fig. 5. During the deformation of the composite scaffolds, three phases were indicated with the stress-strain curve which was elastic region (linear deformation stage), stable stage (plateau) and final stage that the stress decreased rapidly. The tensile strength values of the 12 wt%PVA/0.25 wt%hBN, 12 wt%PVA/0.25 wt%hBN/0.1 wt%BC, and 12 wt%PVA/0.25 wt%hBN/0.5 wt%BC composite scaffolds were higher than that of 12 wt%PVA. On the other hand, the tensile strength value of the 12 wt%PVA/0.25 wt%hBN/0.25 wt%BC composite scaffold was lower than 12 wt%PVA, but it has a huge standard deviation which may be due to different extrusion speeds of the prepared scaffolds (0.8 mL/h). Elongation at break values had generally increased with the incorporation of the additives as can be seen from Table 1. Bacterial cellulose and hBN increased the ductile nature of the scaffolds. Reason for this can be not only due to hydrogen bonds owing to intraaction of deposited gel but the interaction between deposited layers [8,9].

3.6. Swelling behaviours of the scaffolds

The swelling behaviour of the composite scaffolds was shown in Fig. 6. According to the results, the maximum swelling degree was observed for 12 wt%PVA. Other composites also exhibited an increased swelling degree during the time up to 5th day. However, these values were lower than the matrix polymer (12 wt%PVA). It can be realized that swelling degree of BC free composites of 12 wt%PVA was higher than of the BC added composites. Also, hBN addition, as in the literature, increased the swelling properties when compared to BC added cases [8]. It was also observed that swelling degree increased with time for the first 120 h and then presented a decreasing tendency until the end of the experiment (168 h). In the bacterial cellulose additive groups, the swelling degree decreased with the increased amount of bacterial cellulose. The reason for this tendency could be the number of free spaces into 12 wt%PVA/0.25 wt%hBN composite scaffolds, because the free spaces within the matrix may be decreased with the incorporation of BC that were released during the uptake of the water inside the printed filaments. The high rigid structure in BC content groups not only decreases the water absorption and permeation but also limited the swelling behaviour of materials [27]. The reason for this decreasing behaviour might be due to strong intramolecular bonds occurred between functional groups of PVA and BC [28].

3.7. Biocompatibility results of the scaffolds

After 72 h incubation of human osteoblast cells on 3D tissue scaffolds, in vitro biological properties were examined by cytotoxicity and cell-tissue scaffold interaction. The biocompatibility of the scaffold is a significant property for cellular activity. Thus it must not show toxic effects to the host tissues [12]. The result of the MTT assay was presented in Fig. 7. Human osteoblast cells exhibited increased proliferation and better extracellular matrix compatibility at 12 wt%PVA/0.25 wt%hBN/0.5 wt%BC composite scaffolds compared to the 12 wt%PVA. There was observed no significant change in cell viability with the addition of 0.25 wt%hBN to the 12 wt%PVA composite scaffold. Cell viability was reduced by adding 0.1 and 0.25 wt%BC into the 12 wt%PVA/0.25 wt%hBN composite scaffold. A significant increase in cell viability was observed by increasing the concentration of BC to 0.5 wt% (Fig. 7).

The cell-scaffold interactions were shown in Fig. 8. After 72 h incubation, the morphological structures of the cells attached to the scaffolds were demonstrated by SEM analysis. Osteoblast cells on 12 wt% PVA, 12 wt%PVA/0.25 wt%hBN, 12 wt%PVA/0.25 wt%hBN/0.25 wt%BC, and 12 wt%PVA/0.25 wt%hBN/0.5 wt%BC composite scaffolds appeared to have a rounded morphology (Fig. 8 (a,b, c, d, g, h, i, j) [29]. Cells cultured on scaffolds with the addition of the 0.1 wt% amount of BC appeared to adhere and tended to well spread on the surface using their pseudopodia (Fig. 8 (e, f)) [30,31]. This could be due to the change of hydrophilicity, or additional hydroxyl groups attracted cells to adhere [32]. As a result, it has been shown that BC doped tissue scaffolds can form a natural three-dimensional extracellular scaffold suitable for human osteoblast cells.

4. Conclusions

In this study, the effects of incorporation of bacterial cellulose into the host 12 wt%PVA/0.25 wt%hBN composite scaffolds in different ratios

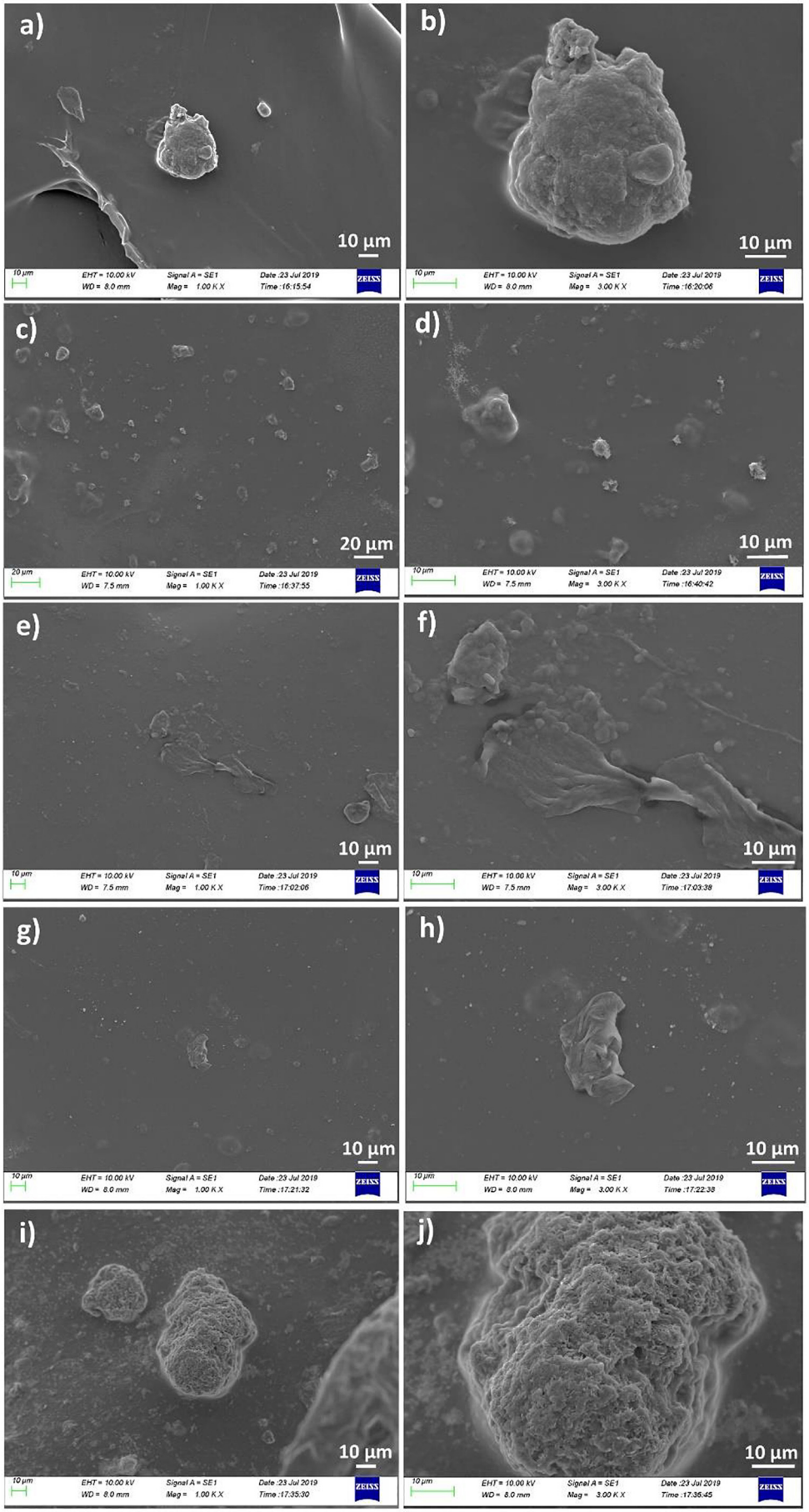


Fig. 8. SEM images of human osteoblast cell cultured on 3D composite scaffolds, 12 wt%PVA (a,b), 12 wt%PVA/0.25 wt%hBN (c, d), 12 wt%PVA/0.25 wt%hBN/0.1 wt%BC (e,f),12wt%PVA/0.25wt%hBN/0.25 wt%BC(g, *h*)and12wt%PVA/0.25 wt%hBN/0.5 wt%BC (i, j) at different magnifications.

were examined. It was observed that the desired pore sizes and the homogeneous scaffold structures were obtained with three-dimensional printing of the polymeric blends. According to DSC analysis, it was found that additive materials did not disrupt the crystal structure of PVA. The significant increase was observed in the cell viability of the structures with 0.5 wt%BC. In view of all the results, the bacterial cellulose doped porous tissue scaffolds were produced successfully with the 3D printing process. The 3D printed functional scaffolds of PVA enhanced with hBN and BC would be an appropriate extracellular matrix structure for bone cells.

Declaration of Competing Interest

The authors declare that they have no known competing financial interests or personal relationships that could have appeared to influence the work reported in this paper.

Appendix A. Supplementary data

Supplementary data to this article can be found online at https://doi.org/10.1016/j.matdes.2020.109094.

References

[1] Z. Sheikh, S. Najee, Z. Khurshid, V. Verma, H. Rashid, M. Glogauer, Biodegradable materials for bone repair and tissue engineering applications, Materials (Basel) 8 (2015) 5744–5794.

[2] X. Lia, S. Lu, Y. Zhuo, C. Winter, W. Xu, B. Li, Y. Wang, Bone physiology, biomaterial and the effect of mechanical/physical microenvironment on MSC Osteogenesis: a tribute to Shu Chien's 80th birthday, Cell. Mol. Bioeng. 4 (2011) 579–590.

[3] A.R. Amini, C.T. Laurencin, S.P. Nukavarapu, Bone tissue engineering: recent advances and challenges, Crit. Rev. Biomed. Eng. 40 (2012) 363–408.

[4] H. Ma, C. Feng, J. Chang, C. Wu, 3D-printed bioceramic scaffolds: from bone tissue engineering to tumor therapy, Acta Biomater. (2018) 37–59.

[5] J.W. Lee, 3D Nanoprinting technologies for tissue engineering applications, J. Nanomater. (2015) 1–14.

[6] A. Butscher, M. Bohner, S. Hofmann, L. Gauckler, R. Müller, Structural and material approaches to bone tissue engineeringin powder-based three-dimensional printing, Acta Biomater. 7 (2011) 907–920.

[7] H. Shao, J. He, T. Lin, Z. Zhang, Y. Zhang, S. Liu, 3D gel-printing of hydroxyapatite scaffold for bone tissue engineering, Ceram. Int. 45 (2019) 1163–1170.

[8] R. Li, J. Lin, Y. Fang, C. Yu, J. Zhang, Y. Xue, Z. Liu, J. Zhang, C. Tang, Y. Huang, Porous boron nitride nanofibers/PVA hydrogels with improved mechanical property and thermal stability, Ceram. Int. 44 (2018) 22439–22444.

[9] M. Zaborowska, A. Bodin, H. Bäckdahl, J. Popp, A. Goldstein, P. Gatenhol, Microporous bacterial cellulose as a potential scaffold for bone regeneration, Acta Biomater. 6 (2010) 2540–2547.

[10] G.F. Picheth, C.L. Pirich, M.R. Sierakowski, M.A. Woehl, C.N. Sakakibara, C.F. Souza, A.A. Martin, R. Silva, R.A. Freitas, Bacterial cellulose in biomedical applications: a review, Int. J. Biol. Macromol. 104 (2017) 97–106.

[11] N. Halib, I. Ahmad, M. Grassi, G. Grassi, The remarkable three-dimensional network structure of bacterial cellulose for tissue engineering applications, Int. J. Pharm. 566 (2019) 631–640.

[12] S. Torgbo, P. Sukyai, Bacterial cellulose-based scaffold materials for bone tissue engineering, Appl. Mater. Today 11 (2018) 34–49.

[13] C. Shuai, Z. Mao, H. Lu, Y. Nie, H. Hu, S. Peng, Fabrication of porous polyvinyl alcohol scaffold for bone tissue engineering via selective laser sintering, Biofabrication 5 (2013), 015014.

[14] H. Awada, C. Daneault, Chemical modification of poly(vinyl alcohol) in water, Appl. Sci. 5 (2015) 840–850.

[15] X. Wang, Y. Xie, Q. Guo, Synthesis of high quality inorganic fullerene-like BN hollow spheres via a simple chemical route, Chem. Commun. (2003) 2688–2689.

[16] R. Auta, G. Adamus, M. Kwiecien, I. Radecka, P. Hooley, Production and characterization of bacterial cellulose before and after enzymatic hydrolysis, Afr. J. Biotechnol. 16 (2017) 470–482.

[17] L.M. Guiney, N.D. Mansukhani, A.E. Jakus, S.G. Wallace, R.N. Shah, M.C. Hersam, Three-dimensional printing of cytocompatible, thermally conductive hexagonal boron nitride nanocomposites, Nano Letters 18 (2018) 3488–3493.

[18] S. Nuernberger, N. Cyran, C. Albrecht, H. Redl, V. Vécsei, S. Marlovits, The influence of scaffold architecture on chondrocyte distribution and behavior in matrix-associated chondrocyte transplantation grafts, Biomaterials 32 (2011) 1032–1040.

[19] D.W. Hutmacher, Scaffolds in tissue engineering bone and cartilage, Biomaterials 21 (2000) 2529–2543.

[20] Z. Qin, L. Hongxu, K. Naoki, Ch. Guoping, Pore size effect of collagen scaffolds on cartilage regeneration, Acta Biomater. 10 (2014) 2005–2013.

[21] A. Sionkowska, A. Płanecka, J. Kozłowska, J. Skopińska-Wiśniewska, Study on the thermal properties of poly(vinyl alcohol) in the presence of collagen, Copernican Lett. 1 (2010), 2082968X.

[22] N. Chen, L. Li, Q. Wang, New technology for thermal processing of poly(vinyl alcohol), Plastics Rubber Compos. 36 (2007) 283–290.

[23] H. Celebi, M. Gurbuz, S. Koparal, A. Dogan, Development of antibacterial electrospun chitosan/poly(vinyl alcohol) nanofibers containing silver incorporated HAP nanoparticles, Compos. Interfaces 20 (2013) 799–812.

[24] M. Mohsen-Nia, H. Modarress, Viscometric study of aqueous poly(vinyl alcohol) (PVA) solutions as a binder in adhesive formulations, J. Adhesion Sci. Technol. 20 (2006) 1273–1280.

[25] P. Phuhongsung, M. Zhang, S. Devahastin, Investigation on 3D printing ability of soybean protein isolate gels and correlations with their rheological and textural properties via LF-NMR spectroscopic characteristics, LWT 122 (2020) 109019.

[26] E. Ilhan, S. Cesur, E. Guler, F. Topal, D. Albayrak, M.M. Guncu, M.E. Cam, T. Taskin, H.T. Sasmazel, B. Aksu, F.N. Oktar, O. Gunduz, Development of Satureja cuneifolia-loaded sodium alginate/polyethylene glycol scaffolds produced by 3D-printing technology as a diabetic wound dressing material, Int. J. Biol. Macromol. 161 (2020) 1040–1054.

[27] W. Treesuppharat, P. Rojanapanthu, C. Siangsanoh, H. Manuspiya, S. Ummartyotin, Synthesis and characterization of bacterial cellulose and gelatin-based hydrogel composites for drug-delivery systems, Appl. Biotechnol. Rep. 15 (2017) 84–91.

[28] T. Jayaramudu, H.U. Ko, L. Zhai, Y. Li, J. Kim, Preparation and characterization of hydrogels from polyvinyl alcohol and cellulose and their electroactive behavior, Soft Mater. 15 (2017).

[29] J.V. Kumbhar, S.H. Jadhav, D.S. Bodas, A. Barhanpurkar-Naik, M.R. Wani, K.M. Paknikar, J.M. Rajwade, In vitro and in vivo studies of a novel bacterial cellulose-based acellular bilayer nanocomposite scaffold for the repair of osteochondral defects, Int. J. Nanomedicine 12 (2017) 6437–6459.

[30] B. Fang, Y.Z. Wan, T.T. Tang, C. Gao, K.R. Dai, Proliferation and osteoblastic differentiation of human bone marrow stromal cells on hydroxyapatite/bacterial cellulose nanocomposite scaffolds, Tissue Eng. Part A 15 (2009) 1091–1098.

[31] E. Altun, M.O. Aydogdu, F. Koc, M. Crabbe-Mann, F. Brako, R. Kaur-Matharu, G. Ozen, S.E. Kuruca, U. Edirisinghe, O. Gunduz, M. Edirisinghe, Novel making of bacterial cellulose blended polymeric fiber bandages, Macromol. Mater. Eng. 303 (2018) 1700607.

[32] D. Kalaskar, J.E. Gough, R.V. Ulijn, W.W. Sampson, D.J. Scurr, F.J. Rutten, S.J. Eichhorn, Controlling cell morphology on amino acid-modified cellulose, Soft Matter 4 (2008) 1059–1065.